



Since January 2020 Elsevier has created a COVID-19 resource centre with free information in English and Mandarin on the novel coronavirus COVID-19. The COVID-19 resource centre is hosted on Elsevier Connect, the company's public news and information website.

Elsevier hereby grants permission to make all its COVID-19-related research that is available on the COVID-19 resource centre - including this research content - immediately available in PubMed Central and other publicly funded repositories, such as the WHO COVID database with rights for unrestricted research re-use and analyses in any form or by any means with acknowledgement of the original source. These permissions are granted for free by Elsevier for as long as the COVID-19 resource centre remains active.



## Molecular docking studies of HIV TAT and sitagliptin nano-formula as potential therapeutic targeting SARS-CoV2 protease



Hani Z. Asfour<sup>a</sup>, Nabil A. Alhakamy<sup>b,\*</sup>, Khalid Eljaaly<sup>c,d</sup>, Ahmed L. Alaofi<sup>e</sup>, Mohamed A. Tantawy<sup>f,g</sup>, Khulood S. Hussein<sup>h</sup>, Ahmed A. Aldarmahi<sup>i</sup>, Mahmoud A. Elfaky<sup>j</sup>

<sup>a</sup> Department of Medical Microbiology and Parasitology, Faculty of Medicine, King Abdulaziz University, Jeddah, 21589, Saudi Arabia

<sup>b</sup> Department of Pharmaceutics, Faculty of Pharmacy, King Abdulaziz University, Jeddah, 21589, Saudi Arabia

<sup>c</sup> Department of Pharmacy Practice, Faculty of Pharmacy, King Abdulaziz University, Jeddah, 21589, Saudi Arabia

<sup>d</sup> Pharmacy Practice and Science Department, College of Pharmacy, University of Arizona, Tucson, AZ, USA

<sup>e</sup> Department of Pharmaceutics, College of Pharmacy, King Saud University, Riyadh, Saudi Arabia

<sup>f</sup> Stem Cells Lab, Center of Excellence for Advanced Sciences, National Research Centre, Dokki, Cairo, Egypt

<sup>g</sup> Hormones Department, Medical Research Division, National Research Centre, Cairo, Egypt

<sup>h</sup> Department of Physiology, Faculty of Medicine-King AbdulAziz University, Jeddah, Saudi Arabia

<sup>i</sup> College of Sciences and Health Professions, King Saud Bin Abdulaziz University for Health Sciences, Makkah - Jeddah Hwy, King Abdul Aziz Medical City, Jeddah, 22384, Saudi Arabia

<sup>j</sup> Department of Natural Products and Alternative Medicine, Faculty of Pharmacy, King Abdulaziz University, Jeddah, 21589, Saudi Arabia

### ARTICLE INFO

#### Keywords:

COVID-19  
DPP4 inhibitors  
Pneumonia  
Nanoparticles  
SARS-CoV-2

### ABSTRACT

The outbreak of COVID-19 pandemic regarded as a major health/economic hazard. The importance of coming up with mechanisms for preventing or treating SARS-CoV-2infection has been felt across the world. This work aimed at examining the efficiency of Sitagliptin (SIT) and human immunodeficiency virus type 1 (HIV-1) *trans*-activator transcription peptide (TAT) against SARS-CoV-2 virus. 3CL-protease inhibition activity and docking studies were examined. According to the results, the prepared complex's formula was as follows 1: 1 SIT: TAT molar ratio, whereas zeta potential and particle size values were at 34.17 mV and 97.19 nm, respectively. This combination did exhibit its antiviral potentiality against SARS-CoV-2 via IC50 values of 9.083 5.415, and 16.14 μM for TAT, SIT-TAT, and SIT, respectively. In addition, the complex SIT-TAT showed a significant ( $P < 0.001$ ) viral-3CL-protease inhibitory effect. This was further confirmed via *in silico* study. Molecular docking investigation has shown promising binding affinity of the formula components towards SARS-CoV-2 main protease (3-CL).

### 1. Introduction

The dipeptidyl peptidase-4 (DPP4) is expressed in many tissues and cell types, including kidney, intestine, liver, thymocytes, and several cells of hematopoietic lineage [1]. DPP4 is not a possible receptor for SARS-COV-2 entry [2]. However, the prolonged and excessive cytokine responses that are noted in COVID-19 patients can be decreased by Sitagliptin (SIT) [3–5]. SIT is anti-diabetic drug used to decrease incertins, which by its turn increase insulin re-lease leading to decreasing blood sugar [6]. A possible immuno-modulatory effect of SIT was seen in the plasma C-Reactive Protein (CRP) and procalcitonin reduction process [7–9]. Type 2 diabetic patients who have been diagnosed with COVID-19

are recently said to have developed even bad outcomes due to poor glucose control in their bodies [7,10]. Humoral and cellular immunity alterations which are age dependent can lead to a rise in the viral replication and a longer suffering from inflammation which could be indirectly the reason for poor death outcomes and some of these changes can be managed by the Dipeptidyl-peptidase 4 (DPP4) Inhibitors like SIT [11–13]. An intriguing fact is that these inhibitors up-regulate the soluble DPP4 plasma levels, but this is separated from the inflammation and it's extent, and can also be one more mechanism by which the SIT could have optimal effects [7,14]. The researchers used an integrative bioinformatics method that began with a search of the biomedical literature for high-confidence SIT-protein/gene connections, then moved on to

\* Corresponding author.

E-mail addresses: [hasfour@kau.edu.sa](mailto:hasfour@kau.edu.sa) (H.Z. Asfour), [nalhakamy@kau.edu.sa](mailto:nalhakamy@kau.edu.sa), [uahmedkaedu.sa@kau.edu.sa](mailto:uahmedkaedu.sa@kau.edu.sa) (N.A. Alhakamy), [keljaaly@kau.edu.sa](mailto:keljaaly@kau.edu.sa) (K. Eljaaly), [ahmedofi@ksu.edu.sa](mailto:ahmedofi@ksu.edu.sa) (A.L. Alaofi), [mohamed\\_tantawy@daad-alumni.de](mailto:mohamed_tantawy@daad-alumni.de) (M.A. Tantawy), [khussein@kau.edu.sa](mailto:khussein@kau.edu.sa) (K.S. Hussein), [aldarmahia@ksau-hs.edu.sa](mailto:aldarmahia@ksau-hs.edu.sa) (A.A. Aldarmahi).

<https://doi.org/10.1016/j.jics.2021.100119>

Received 2 June 2021; Received in revised form 17 July 2021; Accepted 26 July 2021

0019-4522/© 2021 Indian Chemical Society. Published by Elsevier B.V. All rights reserved.

functional analysis utilizing network analysis and pathway enrichment. As a result of the findings, we propose SIT as a putative target for COVID-19 treatment since the identified DPP4 networks are substantially enriched in viral activities essential for viral entrance and infection.

Being combined with cell-penetrating peptides (CPPs), the efficiency and cellular uptake of the anti-COVID-19 medicines can be improved [15–18]. CPPs have less than 30 amino acid residues [19,20]. They are capable of crossing cell membranes by emitting minimal toxicity through energy dependent/independent mechanisms, and even not needing any specific chiral recognition [21]. CPPs being merged with drug molecules has been the main anti-viral technique for CPPs and a few CPPs have gone to the extent of demonstrating anti-viral features [17,22,23]. The human immunodeficiency virus type 1 (HIV-1) has the ability to penetrate cells. The Trans-Activator Transcription peptide (TAT) of HIV1 has set off a whole generation of intra-cellular delivery of loaded therapeutics [24–30]. The TAT peptide which is rich with positively charged amino acids is utilized as a research tool to improve the transport and delivery of the drugs, DNA, proteins, RNA, nanoparticles and viruses in the cytoplasm [24–31]. These anti-COVID-19 drugs' efficacy can be enhanced by associating it with TAT peptide [32]. Evaluating the efficiency and effectiveness of the combination of TAT and SIT against SARS-CoV-2 was the objective of this research, to help open the doors to the research that could help eliminate this pandemic virus. As of now, no medication or vaccine has been successful to treat and cure COVID-19 patients [33]. Hence, this repurposed drug could be an excellent substitute with the ability to fight and possibly defeat this virus.

The aim of this work was to evaluate and the efficiency and effectiveness of the TAT and SIT optimized complex against isolate of SARS-CoV-2.

## 2. Materials and methods

SIT was a gift from jamjoom pharmaceuticals (Jeddah, Saudi Arabia) and human immunodeficiency virus type 1 (HIV-1) *trans*-activator transcription peptide (TAT) was purchased from Chengdu Youngshe Chemical Co., Ltd. (Chengdu Youngshe Chemical Co., Chengdu, China).

### 2.1. Preparation of SIT-TAT formulations

1: 1 SIT: TAT molar ratio are placed, in 20 mL of 0.01 M phosphate buffer pH 5.5 before being whirled for a couple of minutes before its dissolution. A 1 mL aliquot of mixed solutions was diluted in 10 mL of the same buffer to determine the Zeta potential and the size of particles.

#### 2.1.2. Particle size and zeta potential determination

The prepared SIT-TAT formations' nano-particles had been spread throughout the waterbody and measured a particle-size analyser (Zetatrack; Microtrac Inc., Montgomeryville, PA, USA), used to analyze the size of particles and the Zeta potential. Three readings were done to determine the average Zeta potential and size of particles.

#### 2.1.3. TEM investigation of the optimized SIT-TAT complex

SIT-TAT optimized complex dispersion (one drop) was spread on a carbon grid and then phosphotungstic acid was utilized for staining. After that, the sample was dried, and then investigated by TEM (JEM-1011: JEOL, Tokyo, Japan).

#### 2.1.4. FTIR spectroscopy investigation of the optimized SIT-TAT NPs

Another analysis called the FTIR analysis was performed to view the interaction taking place between TAT and SIT spectrums, which was estimated at 4000-400  $\text{cm}^{-1}$  With the help of the FTIR spectrophotometer (Nicolet IZ 10, Thermo Fisher Scientific, Waltham, MA, USA).

### 2.3. In vitro 3CL-protease inhibition test

A fluorescent substrate that harbored the cleavage site of SARSCoV-2

Mpro, SARS-CoV-2 3CL Protease, GenBank Accession No. YP\_009725301, a.a. 1-306, denoted in an expression system of *E. coli*, MW 77.5 kDa, as well as buffer comprising 100 mM NaCl, 20 mM Tris, pH 7.3, and 1 mM EDTA, 1 mM DTT utilized for inhibition assay, MW 507.5 Da was leveraged as control and GC376 a 3CL protease inhibitor. In the cleavage assay based on FRET, the Edans' fluorescence signal formed via a Flx800 fluorescence spectrophotometer owing to the substrate's cleavage by 3CL Protease was observed at an emission wavelength of 460 nm where excitation was 360 nm [34]. To begin with, 30  $\mu\text{L}$  of diluted SARS-CoV-2 3CL Protease was inserted into a 96-well plate that contained test formula's pre-pipetted 10  $\mu\text{L}$ . This was followed by the incubation of the combination at room temperature for 30 min via slow shaking. The reaction was then started by adding 10  $\mu\text{L}$  of substrate dissolved inside the buffer at volume of 50  $\mu\text{L}$  final volume, before being incubated at room temperature for 4 h. After sealing the plates, the measurement of fluorescence intensity was checked in a microtiter plate-reading fluorimeter with a 360 nm wavelength that could detect emissions at 460 nm wavelength [35,36].

### 2.4. Molecular docking studies

The investigation of molecular docking was carried out via the Molecular Operating Environment (MOE) platform. The MOE builder module was used to build the two studied ligands that then underwent energy-minimization through MMFF-mediated partial charges and the gradient used was  $1 \times 10^{-3}$  kcal/Å [37]. These minimized and prepared ligands were subsequently saved in the format of chemical file (Molecular Data Base) so that it could be used in line with the protocol of molecular docking. The biological target was obtained from RCSB-Protein Data Bank (PDB ID: 6LU7) before being prepared within the MOE protein preparation tool, where 3D-protonation and auto-correction for atoms types, connections, and charges were adopted. Thereafter, the binding site was defined by MOE Alpha Site Finder, after which the active site was refined to involve the crucial binding residues reported within current literature. Dummy atoms generated from the obtained alpha spheres were assigned as polar-hydrophobic descriptors of the pre-defined  $\text{M}^{\text{PTO}}$  active site. The MOE rigid docking protocol was adopted based on former analysis of  $\text{M}^{\text{PTO}}$  binding site. The flexibility of Mpro-substrate binding pocket was as both S1' as well as S1 subsites were either too rigid or underwent minor changes at the end [38]. A high correlation of superposition between M-pro's apo- and holo-states of 6M03 and 6LU7, respectively denoted a non-presentable discrepancy between the two states [39,40]. Thus, a non-relevant impact of the local ligand induced-fit effect to  $\text{M}^{\text{PTO}}$  binary complex structure within the macromolecule crystalline states. Taking cues from the docking algorithm, the development of ligand conformations was undertaken via bond rotation, inside the active site in congruence with the triangle matcher approach, before being ranked using the London dG scoring function. The retained number of poses (preset for 10 poses) were then refined by minimizing energy in the pocket before being rescored with GBVI/WSA dG forcefield-based scoring function depending on Coulombic electrostatic using the currently loaded charges, protein-ligand van der Waals score, solvation electrostatic, and exposure-weighted surface area weighted [41,42]. The root-mean-square deviation (RMSD) values were considered to assess the validity of the docking protocol keeping the cut-off below 2.0 Å and 3.0 Å for SIT and the proteinomimetic ligand, HIV-1 TAT protein, respectively. PyMol graphical interface software was used to analyze and visual investigate the interactions involving ligand-protein binding [43].

### 2.5. Statistical analysis

This was done using the IBM SPSS® statistical software (Version 25) procured from Chicago, IL-based SPSS Inc. Both ANOVA as well as Tukey's post were implemented in case multiple comparisons were made. Sets of experiments were reported using Standard Deviation. These experiments were then conducted a minimum of four times prior to

examining the results. p values exceeding 0.5 were deemed significant.

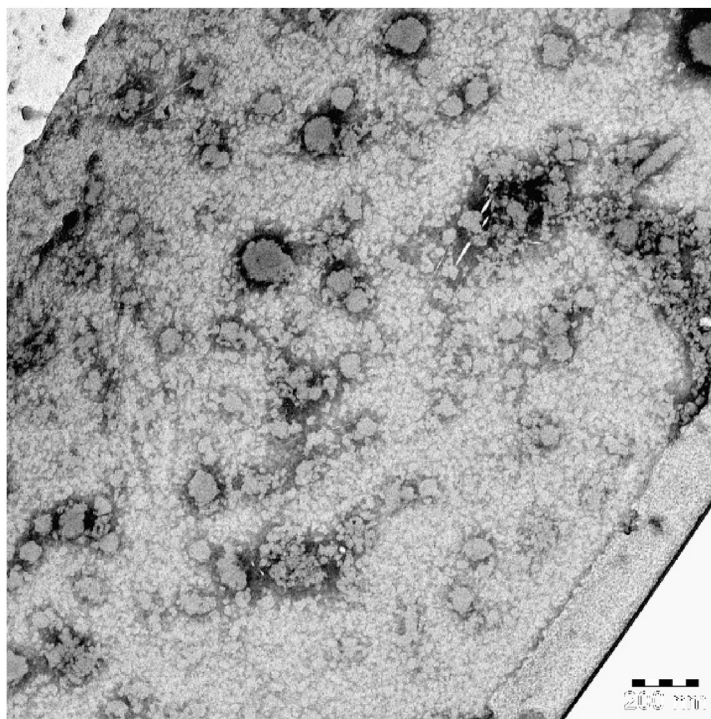
### 3. Results

SIT-TAT nano-formulations were developed according to a full three-factor bi-level ( $2^3$ ) factorial design to obtain the optimized formula. The explored independent variables were SIT concentration (mM, X1), TAT concentration (mM, X2), and pH (X3), while the measured responses were particle size (PS, nm, Y1) and zeta potential (ZP, mV, Y2). The

antiviral activity through testing its inhibition effect on 3-CL main protease. Finally, Molecular docking studies were carried out to interpret the observed enzyme inhibition activities based on drug-protein interactions.

#### 3.1. Transmission electron microscope investigation of the optimized SIT-TAT complex

Transmission electron microscope (TEM) photographs of optimized SIT-TAT complex showed rounded structures revealing some



## II

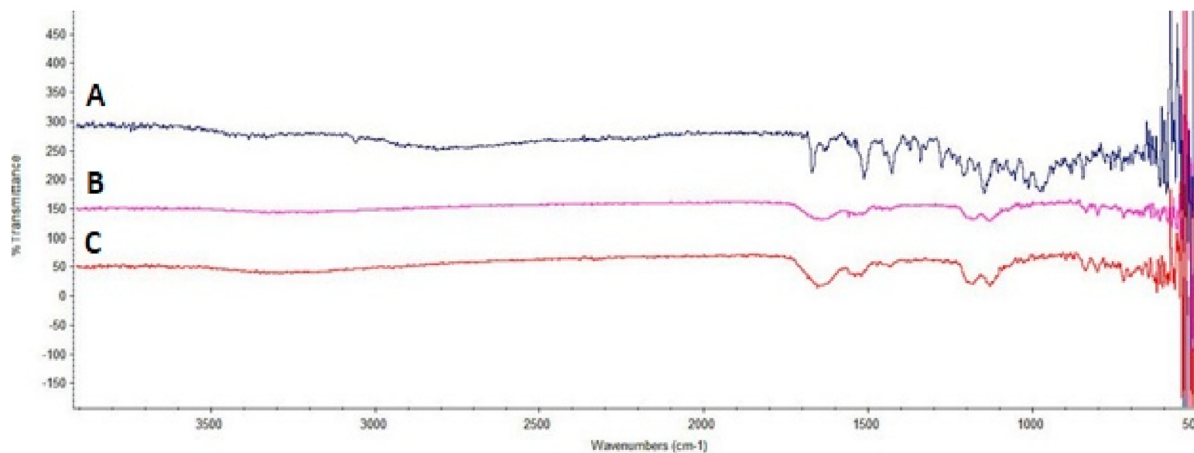


**Fig. 1.** Characterization of the optimized SIT-TAT Complex. I) TEM image of the optimized SIT-TAT Complex (II) FTIR spectra of SIT (A), TAT (B), and combination of SIT-TAT (C).

aggregations potentially caused by the drying process during sample preparation (Fig. 1I).

### 3.2. Fourier-Transform Infrared spectroscopy investigation of the optimized SIT-TAT complex

Fourier-Transformed Infrared (FTIR) investigation as carried out to the interaction taking place between TAT and SIT spectrums, which was estimated at 4000-400  $\text{cm}^{-1}$ . SIT base form displayed band regions which can be categorized in the following manner: 1650-1690  $\text{cm}^{-1}$  is linked to the amidic C=O bond stretching, 1630  $\text{cm}^{-1}$  denotes the Imine C=N bond, 3049  $\text{cm}^{-1}$  aromatic C-H bending, 1570  $\text{cm}^{-1}$  pertains to N-H Bending vibration, 1465  $\text{cm}^{-1}$  pertains to methylene group's C-H bending and 1000-1400  $\text{cm}^{-1}$  vibrations are associated with fluoride, as shown in Figure (1II A). A robust broadband was shown at 3300-3400  $\text{cm}^{-1}$  of NH<sub>2</sub> stretching comprising guanidine and amino groups linked with a 1600-1700  $\text{cm}^{-1}$  peak pertaining to amidic carbonyl group, and broadband associated with NH stretching at 1580-1650  $\text{cm}^{-1}$ , C=N bending of guanidine at 1670  $\text{cm}^{-1}$ , and amidic C=O bending at 1680  $\text{cm}^{-1}$ . The C-O vibrations from TAT's C-terminal amino acid were detected between 1100 and 1250  $\text{cm}^{-1}$ , Figure (1II B). SIT-TAT showed a very broadband nearly flattened at 3000-3700  $\text{cm}^{-1}$ , Figure (1II C). Also, characteristic bands at 1550-1700  $\text{cm}^{-1}$  and 1100-1400  $\text{cm}^{-1}$  of SIT as well as TAT were sharply reduced with respect to intensity, which ascertained the their interaction with each other.

### 3.3. In vitro 3CL-protease inhibition

Due to the 3CLpro essential role in all coronaviruses for its replication, 3CLpro enzymes are essential targets for drug development. Screening of SIT, TAT and combination of SIT-TAT directed at SARS-CoV-2 3CL-protease was undertaken by using the fluorescence resonance energy transfer (FRET) assay as well as GC376 as the positive control. In vitro 3CL-protease inhibition test results show that the complex SIT-TAT has shown a good inhibitory effect against COVID-3CL-protease

(IC<sub>50</sub> = 3.959  $\mu\text{M}$   $\pm$  0.011) (Fig. 2 C). That inhibitory effect was significantly enhanced ( $P < 0.001$ ), in comparison to SIT's individual components (IC<sub>50</sub> = 10.93  $\mu\text{M}$   $\pm$  0.25) and TAT (IC<sub>50</sub> = 8.128  $\mu\text{M}$   $\pm$  0.42) (Fig. 2 A&B).

### 3.4. Molecular docking studies

To derive more insights into obtained in vitro SARS-CoV-2 main proteases (Mpro) inhibition activity, molecular docking studies were conducted to investigate the predicted ligand-protein binding interactions for SIT along with formulation components. The SARS-CoV-2 Mpro binary complex with the irreversible Michael-acceptor peptidomimetic inhibitor, N3 (PDB ID: PRD\_002214) was the adopted atomic crystallized structure for the presented in-silico studies. The crystallized ligand covalently fits within the substrate active site resembling the Mpro natural substrate, which can then prevent further catalysis. Typically, the Mpro binding cavity consists of four crucial clefts or subsites, S1'-S4, corresponding to the P1'-P4 peptide partitions of the natural substrate amino acids (Fig. 3A) [43].

Throughout the presented molecular docking studies, SIT presented relevant accommodation of the target binding site with a significant docking score of ( $S = -5.739$  kcal/mol; RMSD = 1.363 Å). The fused triazolo [4, 3-a] pyrazine ring of the ligand was settled at the S1 subsite and forecasted polar contacts were Gly143 and Ser144 (Fig. 3B). The ring exhibited a close proximity with Cys145, a S1' catalytic dyad, without predicted polar interactions. However, the SIT 3-trifluoromethyl substituent exhibited preferential anchoring at polar side of S1 pocket comprising the hydrophilic residues, His163, Glu166, and His172. Another hydrogen binding was suggested between the carbonyl of SIT aliphatic linker and important residue Gln189 that can further stabilize the ligand at S3 subsite. Finally, the hydrophobic phenyl group at the terminal part of SIT was forecasted to be deeply anchored towards the S1' subsite where a face-to-face sandwiched  $\pi$ - $\pi$  stacking was depicted with the catalytic His41 amino acid. An overlay of SIT binding pose, with the crystallized ligand N3, showed relevant binding poses regarding the

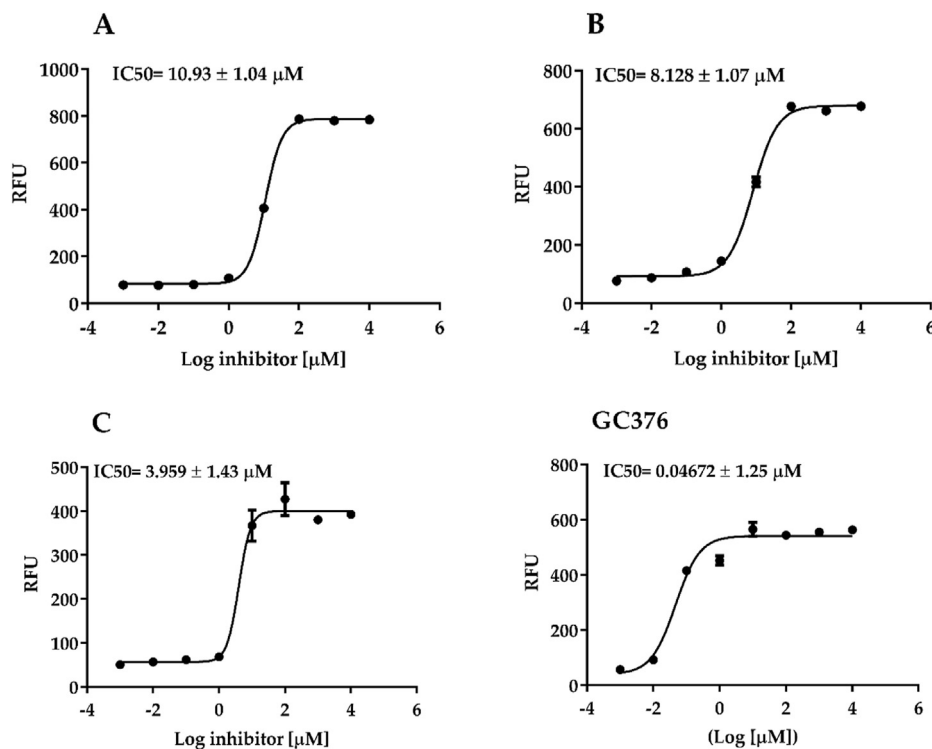
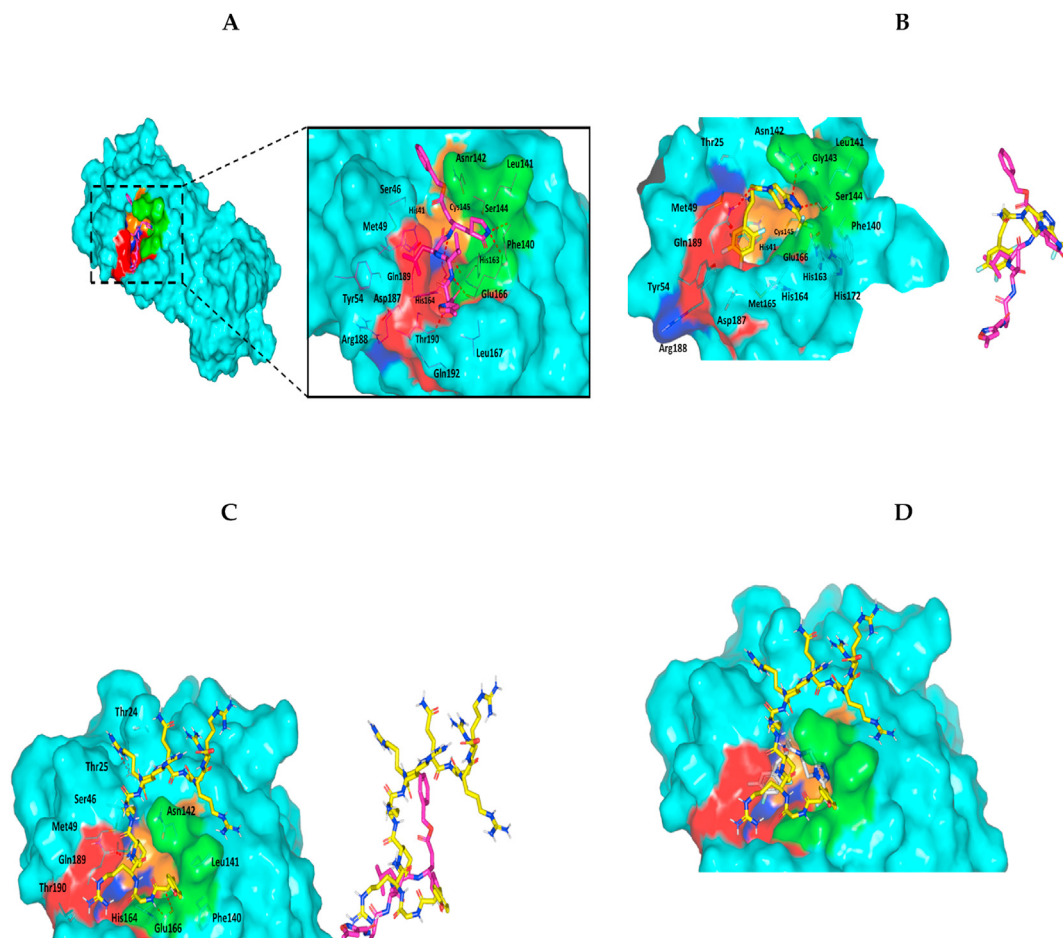


Fig. 2. Inhibition of 3CL Protease enzyme activity by SIT (A), TAT (B), SIT-TAT (C) and control (GC376). Experiment was performed three time ( $n = 3$ ), while the error par presenting SEM.



**Fig. 3.** In silico investigation of the optimized complex. A) Surface 3D-representation of the atom-resolution X-ray diffraction crystallized SARS-CoV-2 main protease (PDB ID: 6LU7; resolution 2.16 Å) in complex with potent inhibitor, N3. The protein biological target is shown in surface 3D-representation with its active site being colored in orange, green, blue, and red, in respective to its subsite pockets (S1', S1, S2, and S3, respectively). Zoomed image is a stereoview of crystallized N3 (magenta sticks) occupying the canonical binding site of Mpro. Polar interactions, represented as hydrogen bonding, are shown as red dashed-lines. Protein's amino acids located within 5 Å radius of ligands are depicted as cyan lines being labeled with sequence numbers. B & C) Predicted docking binding modes of (B) SIT; (C) HIV-1 TAT protein at the SARS-CoV-19 main protease substrate binding site (PDB ID: 6LU7). The predicted binary complexes are represented at the left panels where the protein (surface) is colored representing the pocket's subsite (S1' orange, S1 green, S2 blue, S3 red), while docked ligands are represented as yellow sticks. Right panels illustrate the overlay of docked ligands (yellow sticks) with the crystallized ligand, Michael inhibitor N3 (magenta sticks). Polar interactions, represented as hydrogen bonding, are shown as red dashed-lines. Protein's amino acids located within 5 Å radius of ligands are depicted as cyan lines being labeled with sequence numbers. D) Overlay of docking ligands at the at the SARS-CoV-19 main protease substrate binding site (PDB ID: 6LU7). The target protein (surface) is colored representing the pocket's subsite (S1' orange, S1 green, S2 blue, S3 red), while docked ligands are represented as sticks (yellow for HIV-1 TAT protein and white for SIT). (For interpretation of the references to color in this figure legend, the reader is referred to the Web version of this article.)

ligand's terminal phenyl and fused triazolo[4,3-a]pyrazine scaffolds. The trisubstituted phenyl group depict significant orientation that is comparable to the N3's leucine residue. Meanwhile, the fused triazolo [4, 3-a] pyrazine scaffold predicted comparable orientation at the S1 polar side similar to the pyrrole residue of N.

In terms of the formulation component, TAT exhibited significant accommodation of the binding cavity with a quite higher average docking score ( $S = -6.722$  kcal/mol; RMSD = 2.731 Å) than that of SIT. Due to its greater size, this undeca-peptidomimetic ligand presented relevant anchoring within all pocket subsites of the Mpro substrate binding pocket and adjacent surface clefts (Fig. 3C). Additionally, stabilization of the TAT-protein complex was forecasted via various polar interactions with significant residues. The Glu166 S1 residue contributed in a hydrogen bonding pair with the N-terminal of TAT protein. Double polar interactions were observed between the mainchains of tyrosine-glycine, at the TAT N-terminal, and Glu166 sidechain at S1 pocket subsite. Additionally, both Phe140 and Leu141 showed close proximity to the TAT tyrosine residue, suggesting pertinent hydrophobic interactions for TAT-S1 subsite affinity. In terms of TAT anchoring toward the Mpro

S3 subsite, Gln189 illustrated a significant polar contact with the ligand's lysine residue. It is notable that a double polar interaction with Thr25 sidechain was also exhibited to confirm the reported role of Thr25 for fixing Mpro inhibitors in close proximity to the S1' subsite. An overlay of N3 and TAT conformation depicted minimal superimposition as far as both ligands' C-alpha backbone is concerned, due to the more extended structure of HIV-1 TAT protein. However, the TAT N-terminal arginine residue exhibited great superposed conformation with the proline residue of N3 inhibitor at the S1 subsite. In a similar vein, both the N-terminal arginine of TAT and N3's modified residue (thiazole sidechain) predicted comparable orientation in close proximity to the S3 subpocket.

A comparison of the conformation of both SIT and HIV-1 TAT protein within the target binding site has revealed interesting findings. Despite the fact that both ligands predicted significant accommodation of the Mpro active site, their relative orientations and binding interfaces within the target pocket can be seen to be quite different (Fig. 3D). Owing to its smaller size, SIT suggested deeper anchoring within the target subsites as compared to the undeca-peptidomimetic ligand, HIV-1 TAT. SIT showed greater buried binding mode where residues of both S1 and S3 highly

shield the small ligand molecule from being highly solvent exposed. Separately, the forecasted pose of TAT protein is more confined within the target pocket-solvent interface.

#### 4. Discussion

Another important target is the 3CL protease, as it prevents the replication of the SARS-CoV-2, specifically when it hasn't been located in host cells [44]. The complex of SIT-TAT has an improved inhibitory effect that, with the binding of studied complexes to the active site of 3CL protease, can be justified. The protease showed a competitive inhibition as a result of the strong binding to any such flavonoids, that could in turn result in blocked of enzyme activities [44]. Interestingly, we could prove that SIT and TAT have antiviral activity against an isolate of SARS-CoV-2 which is synergized upon applying the two-component complex. Additionally, the results of the in-silico studies demonstrated strong binding affinity of the drugs to the viral main protease receptor. Most of the predicted ligand/residue interactions came in great agreements with reported studies. Due to the promising advantage of Mpro inhibition to develop effective therapeutics targeting SARS-CoV-2, a plethora of studies identified important target residues, within each subsite. Such interactions have been introduced to impact both small molecule and proteinomimetic ligand binding [38,42,45–47]. Generally, interaction with the Mpro catalytic dyad, (His41 and Cys145) within S1' subsite represent great contribution to strong ligand-protein binding and catalysis inhibition [38]. Additionally, the sidechains of Met165 and Gln189 from S3-subsite as well as His41, Met49, and Asp187 within S2-subsite can provide valuable non-polar interactions serving as the hydrophobic grip pinning ligands to the binding site [38]. Moreover, ligand anchoring at Mpro site can be achieved via hydrophilic interactions with Glu166 mainchain at S1 subsite. Other several relevant residues recognized via different authors are Thr24, Thr25, Pro168, His172, Phe185, and Ala191 [46,48,49].

Within the presented study, both SIT and TAT showed preferential accommodation of the Mpro pockets. Residue-wise interaction with both ligands showed significant polar interaction with Glu166 being responsible for anchoring of many of the reported ligands and introduced as one of the indispensable S1-subpocket residues. The latter confirms the significance of Glu166 binding for fixing both small molecules and proteinomimetic ligands within the Mpro binding site. Only SIT managed to depict relevant contacts with Mpro catalytic dyad which was reasoned for its deep site anchoring owing to its small size. Despite the lack of relevant polar interaction with catalytic dyad, SIT managed to predict significant hydrophobic contact with His41. Such ligand pose suggested a hampering role of SIT small ligands towards the Mpro catalytic machinery being previously introduced by Gimeno and research group [38]. The in-silico study further depicted pocket accommodation of both ligands within Mpro through several polar and hydrophobic contacts with important sub-pocket residues. Significant contacts with S1' Thr25, S1 Phe140, Leu141, Gly143 and Ser144, and/or S3 Gln189 suggested the role of these residues for stabilizing SIT/TAT within the Mpro active site. The latter depicted ligand/pocket residue interaction came in great agreement with several reported studies confirming the significant binding of SIT and TAT at the Mpro pocket [38,42,45–47].

The most interesting in-silico finding introduced within this study, is the ability of both investigated ligands to simultaneously accommodate the Mpro pocket. The deep pocket anchoring of SIT was suggested owing to the ligand's small molecular size as well as its preferential interactions with deep pocket lining residues. On the other hand, the confinement of TAT to the target pocket-solvent interface side was more related to the ligand's extended conformation. However, the extensive polar network and relevant hydrophobic contacts between the TAT protein and relevant pocket residues, of reported role in ligand entrance and binding, can provide evidence for the great stability of TAT at the Mpro active site. Based on the above findings, it is suggested that both SIT and TAT protein can concurrently bind to the SARS-CoV-2 Mpro pocket within a predicted

binding mode being highly stabilized. Moreover, the latter computational behavior of combined formulation of SIT and TAT at the target active site could provide an explanation of the depicted synergistic biological activity of SIT/TAT formulation as compared to sole drug.

#### 5. Conclusions

The SIT-TAT complex showed a promising antiviral activity against isolate of SARS-CoV-2 over its component. In addition to, we explore the mechanism of this activity through testing its inhibition effect on 3-CL main protease. Finally, Molecular docking studies were carried out to interpret the observed enzyme inhibition activities based on drug-protein interactions and results confirm the strong correlation between the synergistic effect of the complex with antiviral findings. Based on the presented findings, an optimized formulation of SIT-TAT could guarantee an enhanced delivery to the target cells, improved cellular uptake, and synergistic blockage of the target active site. The presented findings would guarantee further investigations regarding formula optimization against SARS-CoV-2.

#### Author contributions

Conceptualization, N.A.,H.A. and O.A.; methodology, M.E., U.F.,A.A., M.A., M.T., and T.I.; software, K.H.; validation, N.A., U.F. and A.L.; formal analysis, M.T.; investigation, M.A.; resources, N.A.; data curation,U.F.,K.E.; writing—original draft preparation, K.E.; writing—review and editing, M.E., K.E.; visualization., A.L.,O.A.; supervision, A.A. and H.A.; project administration, M.E.,H.A.,N.A.; funding acquisition, A.L All authors have read and agreed to the published version of the manuscript.”.

#### Funding

This project was funded by the deanship of scientific research (DSR) at King Abdulaziz University, Jeddah under grant N<sup>o</sup> (GCV-19-22-1441). The authors, therefore, acknowledge, with thanks DSR for technical and financial support.

#### Declaration of competing interest

The authors declare that the research was conducted in the absence of any commercial or financial relationships that could be construed as a potential conflict of interest.

#### Acknowledgments

We acknowledge Dr. Ahmed Mostafa, Centre of Scientific Excellence for Influenza Viruses, National Research Centre, Egypt, for technical and scientific assistance during this work. We also thank Dr. Khaled M. Darwish, Medicinal Chemistry Department, Faculty of Pharmacy, Suez Canal University, Ismailia, Egypt, for positive discussions of the in-silico work.

#### References

- [1] Lambeir AM, Durinx C, Scharpé S, De Meester I. Dipeptidyl-peptidase IV from bench to bedside: an update on structural properties, functions, and clinical aspects of the enzyme DPP IV Crit. Rev. Clin. Lab. Sci. 2003;40:209–94.
- [2] Xi CR, Di Fazio A, Nadvi NA, Patel K, Xiang MSW, Zhang HE, Deshpande C, Low JKK, Wang XT, Chen Y, McMillan CLD, Isaacs A, Osborne B, Vieira de Ribeiro AJ, McCaughan GW, Mackay JP, Church WB, Gorrell MD. A Novel Purification Procedure for Active Recombinant Human DPP4 and the Inability of DPP4 to Bind SARS-CoV-2. *Molecules* 2020;25:5392.
- [3] Shu L, Liu Y, Li J, Wu X, Li Y, Huang H. Landscape profiling analysis of DPP4 in malignancies: therapeutic implication for tumor patients with coronavirus disease 2019. *Front. Oncol.* 2021;11.
- [4] Solerte SB, Di Sabatino A, Galli M, Fiorina P. Dipeptidyl peptidase-4 (DPP4) inhibition in COVID-19. *Acta Diabetol* 2020;57:779–83.

- [5] Memis H, Çakır A, Durmus M, Gök S, Bahçecioglu Ö F. Is sitagliptin effective for the treatment of COVID-19? *Eur. J. Hosp. Pharm.* 2021;1.
- [6] Tasyurek HM, Altunbas HA, Balci MK, Sanlioglu S. Incretins: their physiology and application in the treatment of diabetes mellitus. *Diabetes. Metab. Res. Rev* 2014; 30:354–71.
- [7] Mozafari N, Azadi S, Mehdi-Alamdarlou S, Ashrafi H, Azadi A. Inflammation: a bridge between diabetes and COVID-19, and possible management with sitagliptin *Med. Hypotheses* 2020;143:110111.
- [8] Solerte SB, D'Addio F, Trevisan R, Lovati E, Rossi A, Pastore I, Acqua MD, Ippolito E, Scaranna C, Bellante R, Galliani S, Dodesini AR, Lepore G, Geni F, Fiorina RM, Catena E, Corsico A, Colombo R, Mirani M, Riva De C, Oleandri SE, Abdi R, Bonventre JV, Rusconi S, Folli F, Sabatino A Di, Zuccotti G, Galli M, Fiorina P. Sitagliptin treatment at the time of hospitalization was associated with reduced mortality in patients with type 2 diabetes and covid-19: a multicenter case-control retrospective observational study. *Diabetes Care* 2020;43:2999–3006.
- [9] Bardaweel SK, Hajjo R, Sabbah DA. Sitagliptin: a potential drug for the treatment of COVID-19? *Acta Pharm.* 2021;71:175–84.
- [10] Lim S, Bae JH, Kwon HS, Nauck MA. COVID-19 and diabetes mellitus: from pathophysiology to clinical management. *Nat. Rev. Endocrinol.* 2021;17:11–30.
- [11] Bajaj V, Gadi N, Spihlman AP, Wu SC, Choi CH, Moulton VR. Aging, immunity, and COVID-19: How age influences the host immune response to coronavirus infections? *Front. Physiol.* 2021;11:1793.
- [12] Wagner A, Garner-Spitzer E, Jasinska J, Kollaritsch H, Stiasny K, Kundi M, Wiedermann U. Age-related differences in humoral and cellular immune responses after primary immunisation: indications for stratified vaccination schedules. *Sci. For. Rep.* 2018;8:9825.
- [13] Wang X, Zheng P, Huang G, Yang L, Zhou Z. Dipeptidyl peptidase-4(DPP-4) inhibitors: promising new agents for autoimmune diabetes. *Clin. Exp. Med.* 2018; 18:473–80.
- [14] Valencia I, Peiró C, Lorenzo Ó, Sánchez-Ferrer CF, Eckel J, Romacho T. DPP4 and ACE2 in diabetes and COVID-19: therapeutic targets for cardiovascular complications? *Front. Pharmacol.* 2020;11.
- [15] Futaki S, Nakase I. Cell-surface interactions on arginine-rich cell-penetrating peptides allow for multiplex modes of internalization. *Acc. Chem. Res.* 2017;50: 2449–56.
- [16] Desai P, Patlolla RR, Singh M. Interaction of nanoparticles and cell-penetrating peptides with skin for transdermal drug delivery. *Mol. Membr. Biol.* 2010;27: 247–59.
- [17] Silva S, Almeida AJ, Vale N. Combination of cell-penetrating peptides with nanoparticles for therapeutic application: A review. *Biomolecules* 2019;9.
- [18] Allolio C, Magarkar A, Jurkiewicz P, Baxová K, Javanainen M, Mason PE, Sächl R, Cebecauer M, Hof M, Horinek D, Heinz V, Rachel R, Ziegler CM, Schröfel A, Jungvirth P. Arginine-rich cell-penetrating peptides induce membrane multilamellarity and subsequently enter via formation of a fusion pore. *Proc. Natl. Acad. Sci. U. S. A* 2018;115:11923–8.
- [19] Foged C, Nielsen HM. Cell-penetrating peptides for drug delivery across membrane barriers. *Expert Opin. Drug Deliv.* 2008;5:105–17.
- [20] Schmidt N, Mishra A, Lai GH, Wong GCL. Arginine-rich Cell-Penetrating Peptides. *FEBS Lett.* 2010;584:1806–13.
- [21] Kauffman WB, Fuselier T, He J, Wimley WC. Mechanism matters: a taxonomy of cell penetrating peptides. *Trends Biochem. Sci.* 2015;40:749–64.
- [22] Delcroix M, Riley LW. Cell-penetrating peptides for antiviral drug development. *Pharmaceuticals* 2010;3:448–70.
- [23] Pärn K, Eriste E, Langel Ü. The antimicrobial and antiviral applications of cell-penetrating peptides. *Cell-Penetrating Peptides: Methods and Protocols* 2015;1324: 223–45. Springer New York.
- [24] Wang Y, Su W, Li Q, Li C, Wang H, Li Y, Cao Y, Chang J, Zhang L. Preparation and evaluation of lidocaine hydrochloride-loaded TAT-conjugated polymeric liposomes for transdermal delivery. *Int. J. Pharm.* 2013;441:748–56.
- [25] Astriab-fisher A, Sergueev D, Fisher M, Shaw BR, Juliano RL. Conjugates of antisense oligonucleotides with the tat and Peptides : effects on cellular uptake , binding to target sequences , and biologic actions. *Pharm. Res. (N. Y.)* 2002;19: 744–54.
- [26] Alhakamy NA, Fahmy UA, Ahmed OAA. Vitamin E TPGS based transferosomes augmented TAT as a promising delivery system for improved transdermal delivery of raloxifene. *PLoS One* 2019;14.
- [27] Torchilin VP, Levchenko TS. TAT-liposomes: a novel intracellular drug carrier. *Curr. Protein Pept. Sci.* 2003;4:133–40.
- [28] Apte A, Koren E, Koshkaryev A, Torchilin VP. Doxorubicin in TAT peptide-modified multifunctional immunoliposomes demonstrates increased activity against both drug-sensitive and drug-resistant ovarian cancer models. *Canc. Biol. Ther.* 2014;15: 69–80.
- [29] Al-Wahaibi LH, Al-Saleem MSM, Ahmed OAA, Fahmy UA, Alhakamy NA, Eid BG, Abdel-Naim AB, Abdel-Mageed WM, AlRasheed MM, Shazly GA. Optimized conjugation of Fluvastatin to HIV-1 TAT Displays enhanced pro-apoptotic activity in HepG2 cells. *Int. J. Mol. Sci.* 2020;21:4138.
- [30] Park D, Lee JY, Cho HK, Hong WJ, Kim J, Seo H, Choi I, Lee Y, Kim J, Min S-J, Yoon S-H, Hwang JS, Cho KJ, Kim JW. Cell-Penetrating Peptide-Patchy Deformable Polymeric Nanovehicles with Enhanced Cellular Uptake and Transdermal Delivery. *Biomacromolecules* 2018;19:2682–90.
- [31] Zou L, Peng Q, Wang P, Zhou B. Progress in research and application of HIV-1 TAT-Derived cell-penetrating peptide. *J. Membr. Biol.* 2017;250:115–22.
- [32] Ansari MA, Almatroudi A, Alzohairi MA, AlYahya S, Alomary MN, Al-Dossary HA, Alghamdi S. Lipid-based nano delivery of Tat-peptide conjugated drug or vaccine –promising therapeutic strategy for SARS-CoV-2 treatment. *Expert Opin. Drug Deliv.* 2020;17:1671–4.
- [33] Khan Z, Karataş Y, Rahman H. Anti COVID-19 drugs: need for more clinical evidence and global action. *Adv. Ther.* 2020;37:2575–9.
- [34] Zhu L, George S, Schmidt MF, Al-Gharabli SI, Rademann J, Hilgenfeld R. Peptide aldehyde inhibitors challenge the substrate specificity of the SARS-coronavirus main protease. *Antivir. Res.* 2011;92:204–12.
- [35] Wang P, Bai J, Liu X, Wang M, Wang X, Jiang P. Tomatidine inhibits porcine epidemic diarrhea virus replication by targeting 3CL protease. *Vet. Res.* 2020;51.
- [36] Jang M, Park YI, Cha YE, Park R, Namkoong S, Lee JI, Park J. Tea polyphenols EGCG and theaflavin inhibit the activity of SARS-CoV-2 3CL-protease in vitro *evidence-based complement. Alternative Med.* 2020;2020.
- [37] Malebari AM, Ibrahim TS, Salem IM, Salama I, Khayyat AN, Mostafa SM, El-Sabbagh OI, Darwish KM. The anticancer activity for the bumetanide-based analogs via targeting the tumor-associated membrane-bound human Carbonic anhydrase-IX enzyme. *Pharmaceuticals* 2020;13:1–20.
- [38] Gimeno A, Mestres-Truyol J, Ojeda-Montes MJ, Macip G, Saldivar-Espinoza B, Cereto-Massagué A, Pujadas G, Garcia-Vallvé S. Prediction of novel inhibitors of the main protease (M-pro) of SARS-CoV-2 through consensus docking and drug reposition. *Int. J. Mol. Sci.* 2020;21:3793.
- [39] Liang JW, Wang MY, Wang S, Li SL, Li WQ, Meng FH. Identification of novel CDK2 inhibitors by a multistage virtual screening method based on SVM, pharmacophore and docking model. *J. Enzym. Inhib. Med. Chem.* 2020;35:235–44.
- [40] El-Mohsen A, Soliman M, Soliman SS. Protective activities of some extracts from *Euphorbia retusa* leaves towards CCl<sub>4</sub>-induced liver injuries in rats. *Chem. Res. J.* 2020:88–103.
- [41] Mutlu O, Mutluhan Ugurel O, Sariyer E, Ata O, Gul Inci T, Ugurel E, Kocer S, Turgut-Balik D. Targeting SARS-CoV-2 Nsp12/Nsp8 interaction interface with approved and investigational drugs: an in silico structure-based approach *Taylor Fr.* 2020.
- [42] Jin Z, Du X, Xu Y, Deng Y, Liu M, Zhao Y, Zhang B, Li X, Zhang L, Peng C, Duan Y, Yu J, Wang L, Yang K, Liu F, Jiang R, Yang X, You T, Liu X, Yang X, Bai F, Liu H, Liu X, Guddat LW, Xu W, Xiao G, Qin C, Shi Z, Jiang H, Rao Z, Yang H. Structure of Mpro from SARS-CoV-2 and discovery of its inhibitors. *Nature* 2020;582:289–93.
- [43] Tang B, He F, Liu D, Fang M, Wu Z, Xu D. AI-aided design of novel targeted covalent inhibitors against SARS-CoV-2. 2020. *bioRxiv Prepr. Serv. Biol.* 2020.03.03.972133.
- [44] Akaji K, Konno H, Mitsui H, Teruya K, Shimamoto Y, Hattori Y, Ozaki T, Kusunoki M, Sanjoh A. Structure-based design, synthesis, and evaluation of peptide-mimetic SARS 3CL protease inhibitors. *J. Med. Chem.* 2011;54:7962–73.
- [45] Owis AI, El-Hawary MS, El Amir D, Aly OM, Abdelmohsen UR, Kamel MS. Molecular docking reveals the potential of *Salvadora persica* flavonoids to inhibit COVID-19 virus main protease. *RSC Adv.* 2020;10:19570–5.
- [46] Zhang L, Lin D, Sun X, Curth U, Drosten C, Sauerhering L, Becker S, Rox K, Hilgenfeld R. Crystal structure of SARS-CoV-2 main Protease Provides a basis for design of improved a-ketoamide inhibitors. *Science (80-. )* 2020;368:409–12.
- [47] Chen YW, Yiu CPB, Wong KY. Prediction of the SARS-CoV-2 (2019-nCoV) 3C-like protease (3CLpro) structure: virtual screening reveals velpatasvir, ledipasvir, and other drug repurposing candidates. *F1000Research* 2020;9.
- [48] Hung HC, Ke YY, Huang SY, Huang PN, Kung YA, Chang TY, Yen KJ, Peng TT, Chang SE, Huang CT, Tsai YR, Wu SH, Lee SJ, Lin JH, Liu BS, Sung WC, Shih SR, Chen CT, Hsu JTA. Discovery of M protease inhibitors encoded by SARS-CoV-2. *Antimicrob. Agents Chemother.* 2020;64.
- [49] Dai W, Zhang B, Jiang XM, Su H, Li J, Zhao Y, Xie X, Jin Z, Peng J, Liu F, Li C, Li Y, Bai F, Wang H, Cheng X, Cen X, Hu S, Yang X, Wang J, Liu X, Xiao G, Jiang H, Rao Z, Zhang LK, Xu Y, Yang H, Liu H. Structure-based design of antiviral drug candidates targeting the SARS-CoV-2 main protease. *Science (80-) 2020;368:1331–5.*